NUMERICAL RESEARCH OF THE AIR INTAKE LOCATION INFLUENCE ONTO THE HIGH-SPEED AIRCRAFT PERFORMANCE

N.V.Voevodenko*, A.A.Gubanov*
*** TsAGI – Central Aerohydrodynamic Institute, Russia**
nvoevodenko@tsagi.ru; gubanov@ou-link.ru

Abstract

One of the most important questions for high-speed aircraft is efficient airframe-engine integration. For the aerodynamic configuration improvement researches it is necessary the effective, robust, quick and informative tool. Hypersonic Small-Disturbance Theory (HSDT)[1] and Sychov's theory [2] (for high angles of attack) reduces 3D-flow problem and makes CFD-code, based on it, more quick and robust. Numerical code based on HSTD and Godunov-Kolgan numerical method is used as an instrument for calculation of the flow field and total vehicle characteristics.

The air intake performances, such as the intake flow rate, the intake impulse components and so on, are calculated with the aid of method. The impact of air-breathing engine on vehicle aerodynamic performance then could be determined by classical impulse theorem, using flow field parameters on intake entry area, obtained from numerical calculations.

The above code results are compared with RANS-code results and experimental data to verify it.

The data presented here are the results of numerical investigation of the air intake location influence on the aircraft performances and onto the air intake parameters for two different vehicle configurations.

1 Introduction

The actuality of the aerodynamic configuration improvement researches for high-speed aircraft with air-breathing jet engine is caused by the perspective to use such aircraft as the first stage for reusable space transportation systems and also by the development of passenger and business airplanes with high supersonic cruising velocity. One of the most important questions for such aircraft is efficient airframe-engine integration. In this case the favorable choice of the air intake location is one of the key-points for such integration because it has a remarkable influence on the aircraft performances as well as onto the engine performances.

Up-to-date numerical codes permit us to calculate very complex flows around compound airframes, but they request a lot of computational time and resource. Hypersonic Small-Disturbance Theory (alter names: Hayes's theory, unsteady analogy) reduces 3D-flow problem and makes CFD-code, based on it, more quick and robust.

The code for the Euler equation solutions uses the following theoretical and numerical methods:

- HSDT,
- extension of HSDT to the case of high angles of attack (Sychev's theory),
- Godunov-Kolgan's numerical method as the instruments for the small-disturbance theory equations integration.

Basic theory is asymptotic, but in practice it was shown that the applicability range of this method is: $2 \le M_\infty \le 10, |\alpha| < 90°$. Method applicability is verified by the comparison with CFD results (RANS codes) and experimental data.

This methodology and the code based on it give us the ability of the fast and sufficiently informative calculations. One flight regime for one configuration takes about one minute of the ordinary PC. So, a wide airframe variations field

can be quickly calculated to choose the most efficient airframe.

Two different configuration types have been investigated with above tool:

• wing-body airframe with two air intakes,

• axisymmetric body with two air intakes, with the aim to determine the best location of air intakes.

2 Theoretical Basis

The problem of high supersonic flow near the body is considered in ideal-gas approach, so the flow near a three-dimensional (3D) body is described by Euler equations.

To reduce the problem and to make the method more quick and robust the following theoretical basis is used:

• Hypersonic Small-Disturbance Theory - HSDT (alter names: Hayes's theory, unsteady analogy) [1], main assumptions:

$$M_\infty >> 1, \quad \tau \sim \delta = d/L << 1, \quad K = M_\infty \tau \sim 1 \qquad (1)$$

see indications on fig.1,

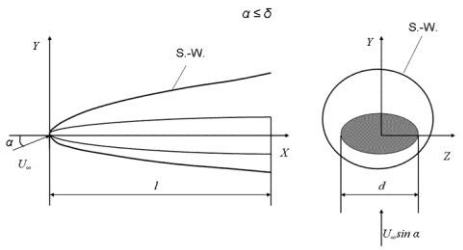

Fig. 1. HSDT - Hayes's theory.

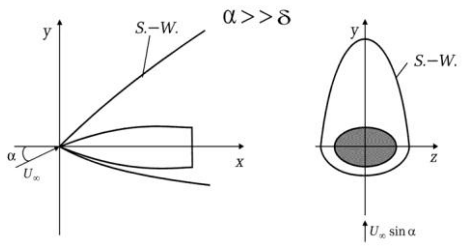

Fig. 2 Sychev's theory

• extension of HSDT to high angles of attack (Sychev's theory) [2], main assumptions:

$$\delta << 1, \quad M_\infty \delta \geq 1, \quad M_\infty \sin\alpha >> 1 \qquad (2)$$

see indications on fig.2.

For small angles of attack theory [2] transforms to theory [1]. The most important parameter, characterizing the precision of theories [1] and [2] is a disturbed flow thickness - τ. For small angles of attack the flow disturbances are confined to a region near the body by the highly swept bow shock wave (fig. 1). For high angles of attack the disturbance field on the compression side of the body will again be confined to a region near the body (fig. 2). But on the leeside the disturbance field will extend a considerable distance. However the leeside field contributes only minimally to the overall loading as long as the compression surface loading is sufficiently high. Hence, the flow-field disturbances of interest are close to the body even for high angles of attack.

Sychev introduced the following dimensionless variables:

$$\begin{aligned} &x = Lx_0, \quad y = dy_0, \quad z = dz_0 \\ &u = U_\infty \cos\alpha \cdot u_0 \\ &v = U_\infty \sin\alpha \cdot v_0 \\ &w = U_\infty \sin\alpha \cdot w_0 \\ &p = \rho_\infty U_\infty^2 \sin^2\alpha \cdot p_0 \\ &\rho = \rho_\infty \rho_0 \end{aligned} \qquad (3)$$

After substitution in 3D Euler equations, then neglecting the values of higher then $o(\delta^2)$-order, and replacing $x_0 = U_\infty \cos\alpha \cdot t_0$, 2D unsteady Euler equations are obtained:

$$\begin{aligned} &\frac{\partial \rho_0}{\partial t_0} + \frac{\partial \rho_0 v_0}{\partial y_0} + \frac{\partial \rho_0 w_0}{\partial z_0} = 0, \\ &\frac{\partial v_0}{\partial t_0} + v_0 \frac{\partial v_0}{\partial y_0} + w_0 \frac{\partial v_0}{\partial z_0} + \frac{1}{\rho_0}\frac{\partial p_0}{\partial y_0} = 0 \\ &\frac{\partial w_0}{\partial t_0} + v_0 \frac{\partial w_0}{\partial y_0} + w_0 \frac{\partial w_0}{\partial z_0} + \frac{1}{\rho_0}\frac{\partial p_0}{\partial z_0} = 0, \\ &\frac{\partial s_0}{\partial t_0} + v_0 \frac{\partial s_0}{\partial y_0} + w_0 \frac{\partial s_0}{\partial z_0} = 0, \end{aligned} \qquad (4)$$

$$s_0 = \frac{p_0}{\rho_0^{æ}}$$

and corresponding conditions on the body surface $f(x_0, y_0, z_0) = 0$:

$$\frac{\partial f}{\partial t_0} + v_0 \frac{\partial f}{\partial y_0} + w_0 \frac{\partial f}{\partial z_0} = 0 \qquad (5)$$

and on the shock wave surface $F(x_0, y_0, z_0) = 0$:

$$\begin{aligned}
&\left[\rho_0 \frac{DF}{Dt_0}\right] = 0, \qquad \left[\rho_0 v_0 \frac{DF}{Dt_0} + p_0 \frac{\partial F}{\partial y_0}\right] = 0, \\
&\left[\rho_0 w_0 \frac{DF}{Dt_0} + p_0 \frac{\partial F}{\partial z_0}\right] = 0 \\
&\left[\rho_0 \frac{DF}{Dt_0}\left(\frac{v_0^2 + w_0^2}{2}\right) + \frac{æ}{æ - 1}\frac{p_0}{\rho_0} + \right. \\
&\left. + p_0\left(v_0 \frac{\partial F}{\partial y_0} + w_0 \frac{\partial F}{\partial z_0}\right)\right] = 0 \\
&\frac{DF}{Dt_0} = \frac{\partial F}{\partial t_0} + v_0 \frac{\partial F}{\partial y_0} + w_0 \frac{\partial F}{\partial z_0}
\end{aligned} \qquad (6)$$

Axis t with origin at the nose tip is aligned along the longitudinal body axis. This is the problem of 2-D unsteady motion of gas caused 2-D piston, which expands and moves on the plane with velocity $U_\infty \sin\alpha$.

So, this theory reduces the 3-D steady Euler equations to the 2-D unsteady Euler equations (the longitudinal coordinate x is replaced by time t, and it is assumed that $u_0 = U_\infty \cos\alpha$). This equation transformation simplifiers the numerical solution of the problem.

3 Numerical Tool

Equations (4) with boundary conditions (5) and (6) are integrated numerically, using Godunov-Kolgan method [3]. The bow shock wave front is determined by procedure [4] and assumed to be a boundary of calculation region. The disturbed region is located between the body surface and the bow shock wave. The calculation grid is attached to the body surface and the bow shock wave. If disturbed region configuration is complex this region is divided into simple subregions. In each subregion the calculation grid is built so that grid points coincide on the boundaries of subregions. Cross section shape determines subregion number and arrangement.

The program can be quickly adjusted for many classes of shapes by creating of corresponding file of geometry.

Name of this code is NINA – Numerical Investigations of Nonlinear Aerodynamics.

This methodology and code based on it gives us the ability of the fast and sufficiently informative calculations. One flight regime for one configuration takes about one minute of the ordinary PC. So, a wide airframe variations field can be quickly calculated to choose the most efficient airframe.

3.1 Methodology of the Aircraft with Air Intake Performances Calculation

The methodology for the aircraft with air intake performances calculation is based on the classical impulse theorem and has a wide application in Russian research institutes.

The total force, acting on the aircraft with air intake, is:

$$\begin{aligned}
&\vec{R}_\Sigma = \vec{R}_A + \vec{T} = \\
&= -\int_{S_w} [(p - p_\infty)\cdot \vec{n}_w + \vec{R}_T]ds + \vec{I}_1 - \vec{I}_c
\end{aligned} \qquad (7)$$

where $\vec{R}_A$ - external aerodynamic force (the integral over external aircraft surface), $\vec{T}$ - thrust, $\vec{I}_1$ - impulse on the air intake, $\vec{I}_c$ - impulse on the nozzle exit. Illustration to the formulas is given on fig. 3.

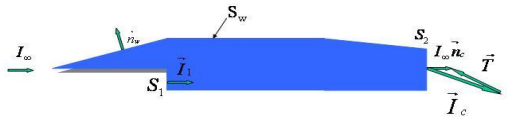

Fig. 3

The engine thrust is determined as:

$$\vec{T} = -\left(\vec{I}_c - |I_\infty|\vec{n}_c\right) \qquad (8)$$

So, external aerodynamic force is:

$$\vec{R}_A = \vec{R}_\Sigma - \vec{T} = \\ = -\int_{S_w} [(p - p_\infty)\cdot \vec{n}_w + \vec{R}_T]ds + \vec{I}_1 - |I_\infty|\vec{n}_c \quad (9)$$

where $I_\infty = V_\infty \int_{S_1} \rho V_x dx, \Rightarrow I_\infty = \rho_\infty V_\infty^2 F_0 f$,

because of

$$\rho_\infty V_\infty F_\infty = \int_{S_1} \rho V_x dx, \Rightarrow f = \frac{F_\infty}{F_0} = \frac{1}{F_0}\cdot\frac{1}{\rho_\infty V_\infty}\int_{S_1}\rho V_x dx$$

F_0 – is the air intake square, F_∞ - the initial jet square, coming to the air intake.

The air intake performances, such as the intake flow rate *f*:

$$f = \frac{1}{\rho_\infty V_\infty F_0}\int_{S_1}\rho V_x ds, \quad (20)$$

the intake impulse components coefficients I_x and I_y:

$$\vec{I}_x = \frac{1}{\rho_\infty V_\infty^2 F_0}\int_{S_1}[(p - p_\infty) + \rho V_x^2]ds \quad (31)$$

$$\vec{I}_y = \frac{1}{\rho_\infty V_\infty^2 F_0}\int_{S_1}\rho V_x V_y ds \quad (42)$$

,

the intake longitudinal moment component coefficient $\vec{m}_z$:

$$\vec{m}_z = \frac{1}{\rho_\infty V_\infty^2 F_0 L_{xap}}\int_{S_1}[(p - p_\infty) + \rho V_x^2]y\, ds \quad (53)$$

and so on, are calculated using the flow field data on the air intake area, obtained by above method. Then for external aerodynamic coefficients calculation we use the following formulas:

$$C_x = C_{xw} - 2\frac{F_0}{S_{xap}}\left(f - \vec{I}_x\right) \quad (63)$$

$$C_y = C_{yw} - 2\frac{F_0}{S_{xap}}\vec{I}_y \quad (74)$$

$$m_z = m_{zw} - 2\frac{F_0}{S_{xap}}\vec{m}_z, \quad (85)$$

where "w" in index means the value on external aircraft surface, S_{xap} - aircraft characteristic area, L_{xap} - aircraft characteristic length.

3 Method Verification

Method was reliably tested before by the comparison with experimental data and other calculation results [5]. Only few examples of the method verification are shown on fig. 4-5:

- Total characteristics of cones - C_x, C_y, M_z and X_g, obtained by this method (solid lines), are compared with experimental data (points) at $M = 7$ and $\alpha = 0° \div 60°$ on fig. 4.

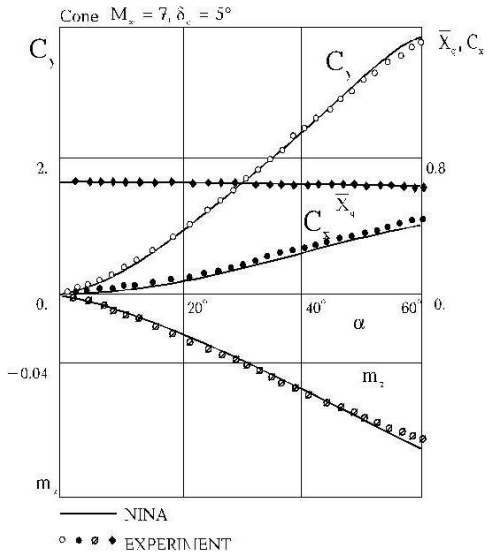

Fig. 4

- Fig. 5 shows C_p distribution on compression side of delta-wing at $M = 6$ $\alpha = 30°, 40°, 50°$. Touch lines are this method results. Other lines are obtained by other calculation methods, points are experimental results.

Additional numerical verification was done by comparison with RANS solution obtained with commercial code NUMECA. The calculations of axisymmetric body with ogival nose (length L=3.), continued by cylinder (diameter D=1. L/D=λ=3), have been performed at Mach numbers M_∞= 3.; 4. and angles of attack α = 0°; 5°; 10° with both – NINA и NUMECA codes. The results have been compared which rise its reliability and is

a kind of verification also. Cross sections of the parameters flow fields, obtained with the tools mentioned above, are shown on fig. 6.

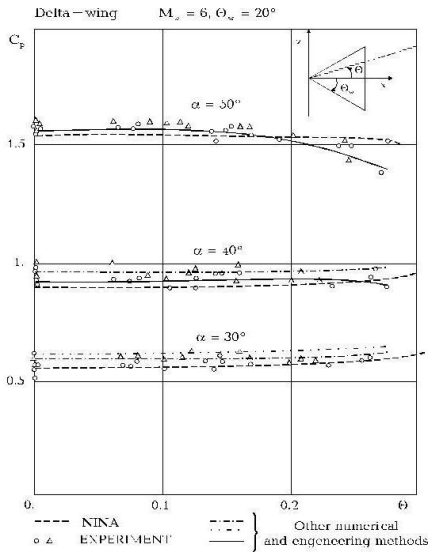

Fig. 5

Here are presented flow fields of Mach number, density and pressure at M_∞= 4. and α = 0° in cross section X=3. On the plot black curves indicate NUMECA results, multicolor curves indicate NINA results. Apparently, the pressure results are close in whole flow field besides region near the shock wave,

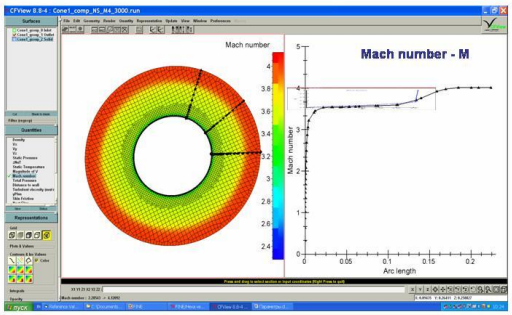

Fig. 6a

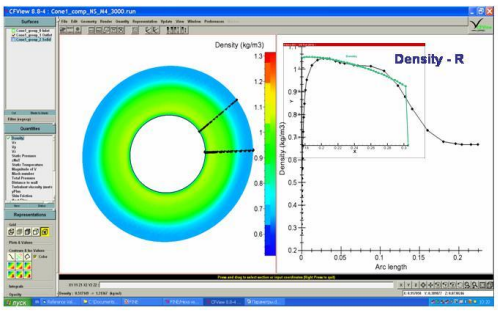

Fig. 6b

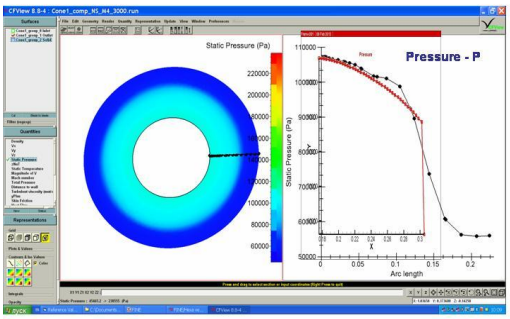

Fig. 6c

surrounding disturbed region. The reason of it is: NINA calculates with the shock wave detection, a NUMECA – with the shock wave capturing technique. Density and local Mach number are in good agreement in central part of field, but differ in boundary layer near body surface and near shock wave also. But in central part of the flow field, where the air intakes are located, the methods give very close results for all parameters influencing on the intake characteristics.

4 Optimization of the air intake location

With the aid of described method we have investigated the influence of the air intake location to the aerodynamic characteristics of the airframe and air intake.

Two different types of the vehicle configurations are considered:

- Body + Delta wing + Two air intakes under wing;
- Axisymmetric body + Two air intakes.

4.1 Application 1

The airframe under consideration has the following main features: delta-wing with half-cone followed by half-cylinder above it and two square air intakes under it, as shown on fig.7.

First stage of investigation was done at fixed flight regime: M_∞ = 4, α = 5°. The aircraft model has 100 dimensionless units length (L=100), air intakes front point is at x=50.

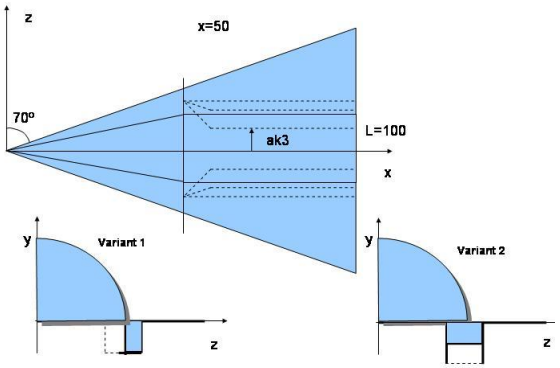

Fig. 7

The geometry variations were:

1. Air intake (of variant 1 – vertical position of the braking wedge, fig.7) displacement along wing span in the cross-section x=50. Calculations with ak3=0.1, 0.2, 0.3, 0.4, 0.5, 0.6 have been performed (ak3= distance between symmetry plane and intake wall / wing span at x=50.). Further displacement to the wing edge is prohibitive because of the bow shock-wave fall on the air intake.
2. Air intake (of variant 2 – horizontal position of the braking wedge, fig.7) displacement along wingspan in the cross-section x=50. Calculations with ak3=0.1, 0.2, 0.3, 0.4, 0.5, 0.6 have been performed.
3. Air intake (of variant 1) displacement along x-axis in the cross-sections x=60. and 70. In these cross-sections we seek to displace air intake closer to wing edge to use the flow angularity to leading edges for improving the air intake performances.

The studies have shown that:

- the air intake displacement from the symmetry plane to the delta wing edge improves the air intake performances. Fig. 8-9: the air intake flow rate *F* – fig. 8, averaged on intake area Mach number *M* – fig. 9, demonstrate the intake performances rising with ak3.
- Variant 1 with vertical position of the braking wedge is much more efficient

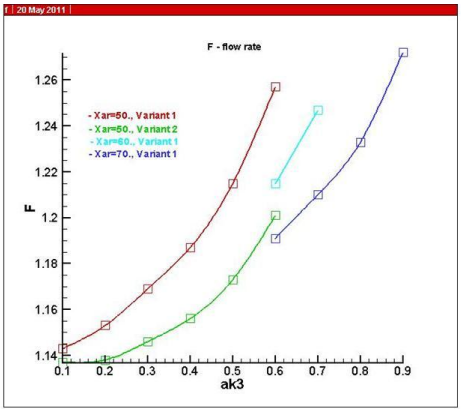

Fig. 8

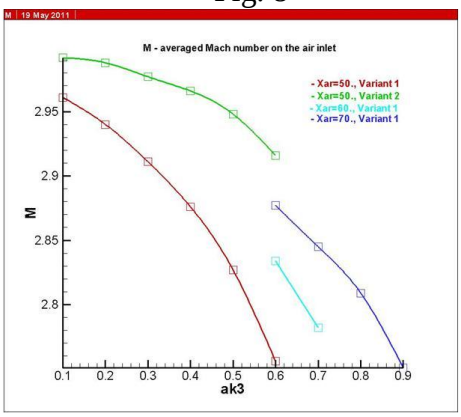

Fig. 9

than variant 2 with horizontal position of the braking wedge.

These effects are explained by physics of flow (flow field pictures – fig.10-13). With displacement to the edges more dense air with flow angularity to leading edges comes to the intake. Vertical braking wedge presses out the angular flow to the center, rising air density and inlet flow rate.

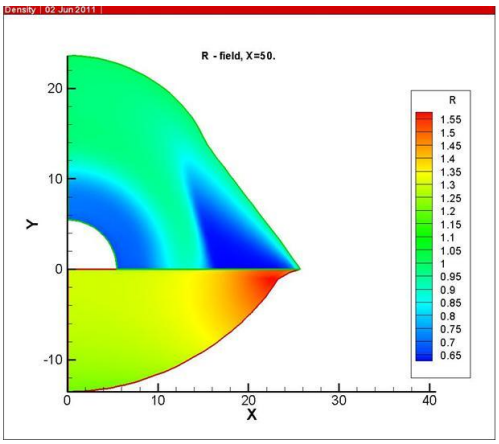

Fig. 10

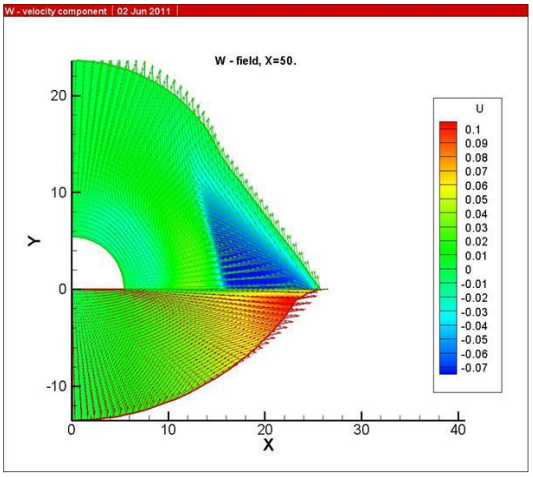

Fig. 11

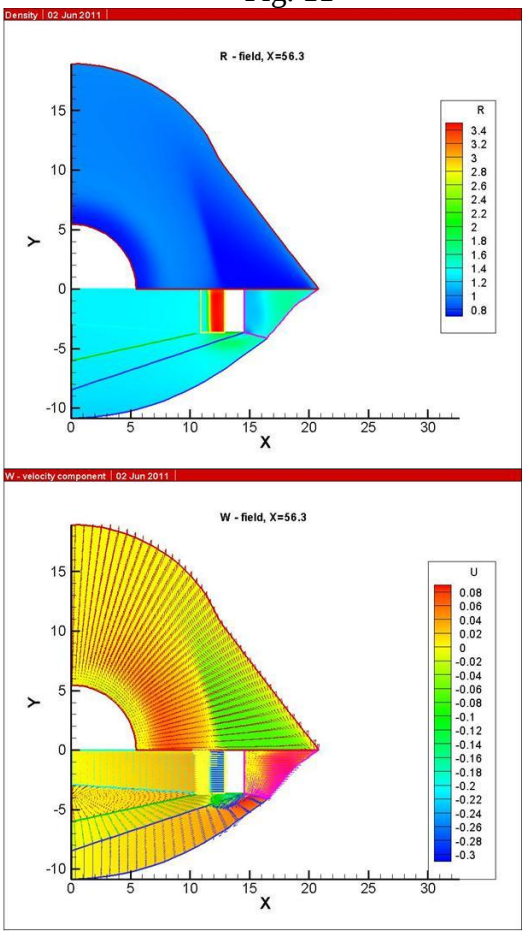

Fig. 12 Flow field for Variant 1.

Total airframe performances aren't very much influenced by the above intake displacements, but the lift-drag ratio (fig.14) is also rising with intake displacement to the wing leading edges.

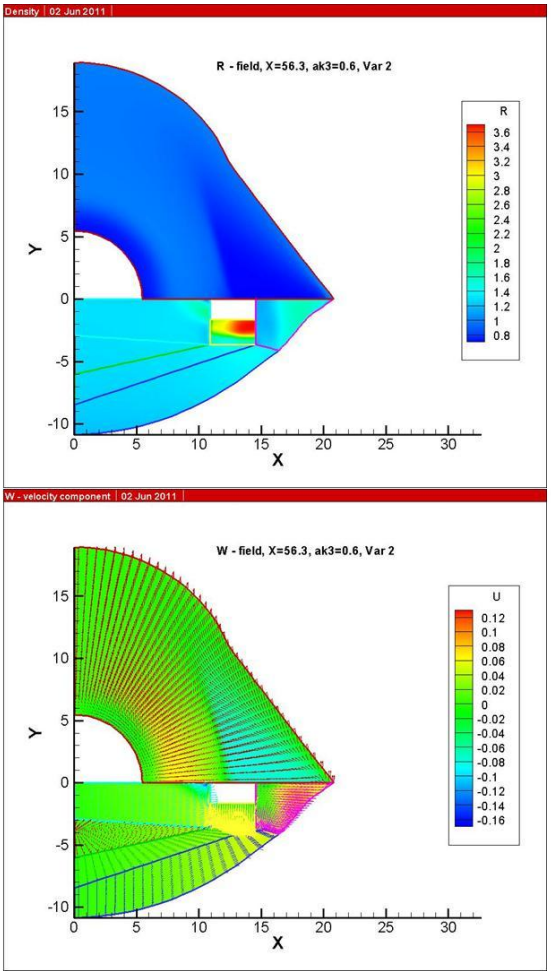

Fig. 13 Flow field for Variant 2.

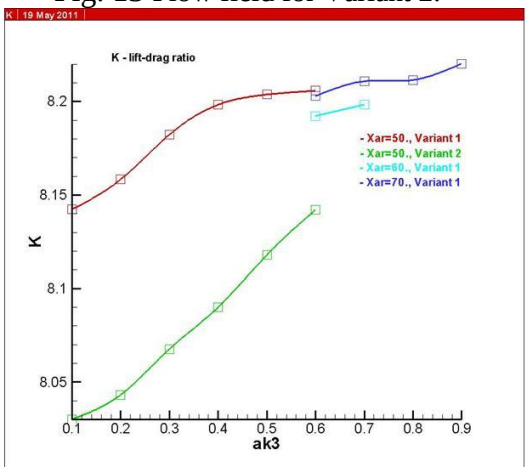

Fig. 14 – Airframe lift-drag ratio K.

4.2 Application 2

Second type of the vehicle configuration considered in this paper is axisymmetric body with two air intakes. The investigation aim is to determine the favorite location of air intakes to provide the best intake performances.

It is reasonable to locate the intakes in the

places with best local characteristics, such as flow rate coefficient, density and where it is possible to use the favorite velocity angles. Apparently, it is the windward side of the flow field. So, the range of the angle φ variation was: 0°≤φ≤75°, see fig. 15.

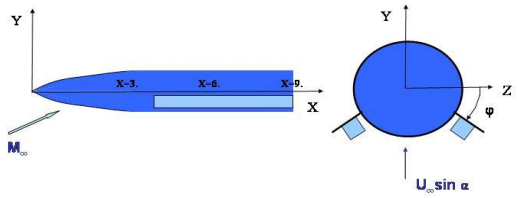

Fig. 15 Application 2 geometry

Nose part of the body has ogived form of length 3., after X=3. body is cylinder of diameter 1.

Air intakes have the square entrance section with side h=0.1. Rectangular plate of width 0.3 is located over the air intake to collect the angular cross flow to provide the flow rate coefficient rising. This plate leading edge is located on the distance 0.5 upwind the air intake.

The air intake position was varied by angle φ from its upper position (φ=0°) till its lower position (φ=75°) on the windward side of flow field, in three cross sections: X = 3.5; 6.5; 9.5.

Calculations were done at Mach number M_∞ = 4. and angle of attack α = 10°. Fig. 16 shows the flow rate coefficient dependence on φ. The curve color correspondence: red - X=3.5, green – X=6.5, blue – X=9.5.

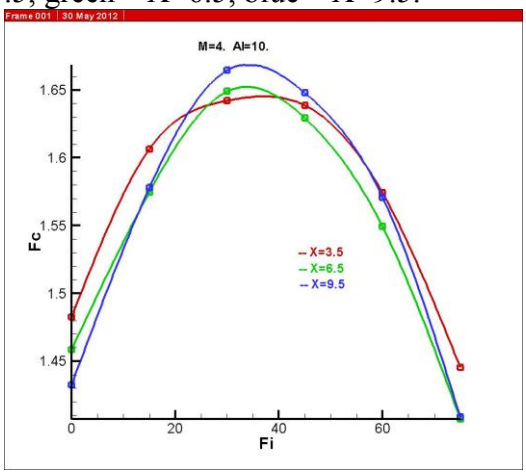

Fig. 16

Apparently, the flow rate coefficient has maximum around φ=35÷40° in all three sections.

Fig. 17 demonstrates pressure and density fields in section X=3.5 for two intake positions closest to the maximum φ=30° and φ=45°.

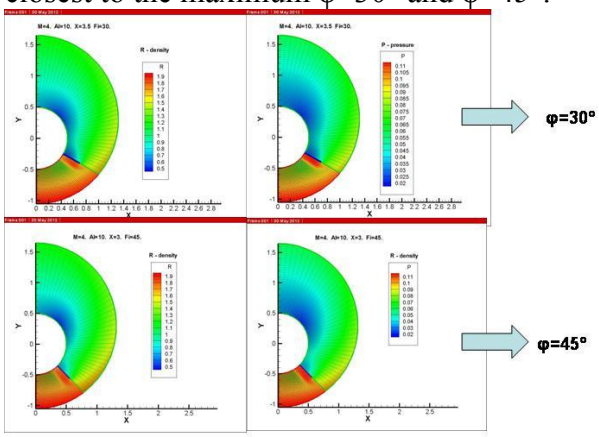

Fig. 17

High pressure and density flow comes to the air intake in these positions due to angular flow collected by plate.

Fig. 18 shows the flow rate coefficient field at X=3.5 for different air intake positions: φ=0°, 15°, 30°, 45°, 60°, 75°. Most high flow rate coefficient is at φ=35÷40°.

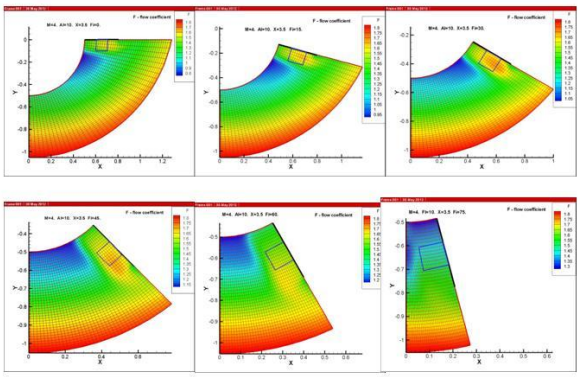

Fig. 18

For quick preliminary estimation of local flow rate coefficient *F*, under plate in the flow field, created by the body, it is possible to use the correction methodology, based on the formulas for oblique shock wave. Fig. 19 illustrates this methodology.

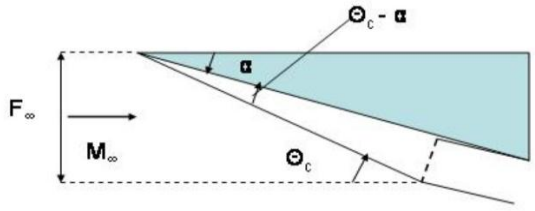

Fig. 19

The parameters correction is performed using the formulas for oblique shock wave generated by plate as it is shown on fig. 19. So, local flow rate coefficient can be recalculated, taking into account the plate influence, by the following formula:

$$f = \frac{\sin\theta_c}{\sin(\theta_c-\alpha)} = \frac{\sin\theta_c}{\sin\theta_c\cos\alpha-\cos\theta_c\sin\alpha} \approx \frac{1}{1-ctg\,\theta_c\cdot\alpha} \approx 1+\alpha_l\sqrt{M_l^2-1}, \quad (16)$$

$$\theta_c = \arcsin\frac{1}{M_l};$$

$$F' = F\cdot f = F(1+\alpha_l\sqrt{M_l^2-1})$$

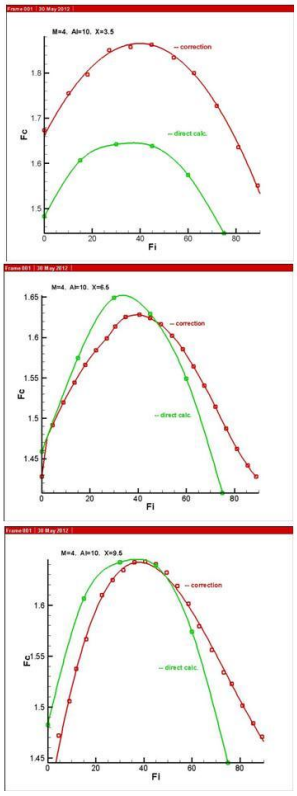

Fig. 20

Fig. 20 demonstrates the direct airframe calculations (green curves) in comparison with results obtained with the correction formulas (16) (red curves) in three cross sections. In section X=3.5. there is significant difference between results, which can be explained by the essential 3D nonuniform flow after ogival nose with longitudinal exhausting, which cannot be taken into account by the correction formulas. In sections X = 6.5 and 9.5, where there is not essential longitudinal exhausting, the results of correction formulas (16) are close to the direct calculations results. Integrally it is possible to conclude that correction methodology (16) can be used for preliminary estimation of the air intake location.

Fig. 21 shows the field of function F' ($FF=F'$), determined by (16), which apparently indicates that this function has maximum near φ=40°.

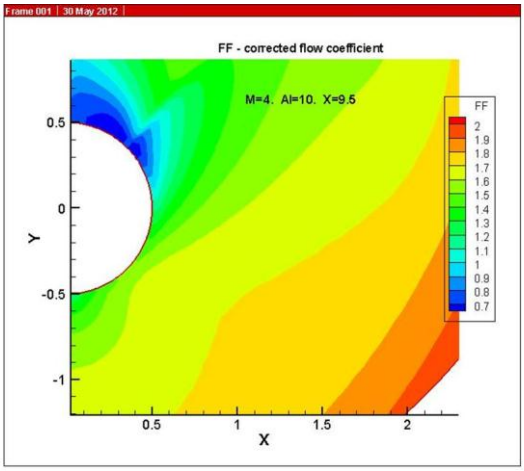

Fig. 21

So, the researches have made it possible to determine the favorite air intake location in the flow field near axisymmetric body: maximum flow rate coefficient is around φ=35÷40° in all cross sections. As for longitudinal location, in the sections fare from nose (X=6.5, 9.5) maximums of flow rate coefficient are very close.

5 Conclusions

1. Numerical investigation of the air intake location influence onto the air intake parameters and on the aircraft performances for two different vehicle configurations have been performed at Mach numbers M_∞= 3.; 4. and small angles of attack.

2. Quick and robust numerical tool, based on Hypersonic Small Disturbance Theory and

Godunov-Kolgan method was used as main research instrument.

3. Method is tested by comparison with experimental results and calculation results of RANS-code, which show the suitable agreement of results.

4. The methodology, based on the classical impulse theorem, is used to calculate the aircraft with air intake performances.

5. The studies of 1st configuration (wing-body airframe with two air intakes) have shown that:

- the air intake displacement from the symmetry plane to the delta wing edge improves the air intake performances,
- the variant with vertical position of the braking wedge is much more efficient than variant with horizontal position of the braking wedge.

6. The studies of 2nd configuration (axisymmetric body with two intakes) have shown that the favorite location of the air intakes is at $\varphi=35\div40°$ and $X \approx 6.5\div9.5$.

References

[1] Hayes W.D. On Hypersonic Similitude. *Quart.Appl.Math.*, V.5, No.1, April 1947.

[2] Sychev V.V. Three-Dimensional Hypersonic Gas Flow Past Slender Bodies at High Angles of Attack. *J.Appl.Math.Mech.*, V.24, No.2, 1960.

[3] Godunov S.K., Zabrodin A.V., Ivanov M.J., Krajko A.N., Prokopov G.P. *Numerical solution of multidimensional gasdynamics problems.* Moscow, "Nauka", 1976.

[4] Krajko A.N., Makarov V.E., Tillajeva N.I. On numerical construction of shock-wave fronts. *Jou. of Num.Math.and Math.Phys.*, V.20, No.3, 1980.

[5] Voevodenko N.V. Computation of Supersonic/Hypersonic Flow Near Complex Configurations. *ICAS-94-5.2.3,* 19th ICAS Congress, Anahime, CA, USA, 1994.

Copyright Statement